31st Annual International Conference of the IEEE EMBS
Minneapolis, Minnesota, USA, September 2-6, 2009

Stretchable Tracks for Laser-Machined Neural Electrode Arrays

Martin Schuettler, *Member, IEEE*, Damir Pfau, Juan S. Ordonez, *Student Member, IEEE*,
Christian Henle, *Student Member, IEEE*, Peter Woias, Thomas Stieglitz, *Senior Member, IEEE*

***Abstract*—An easy and fast method for fabrication of neural electrode arrays is the patterning of platinum foil and spin-on silicone rubber using a laser. However, the mechanical flexibility of such electrode arrays is limited by the integrated tracks that connect the actual electrode sites and the contacts to which wires are welded. Changing the design from straight lines to meanders, the tracks can be stretched to a certain extend defined by the shape of the meanders. Horse-shoe-like designs described by an opening angle $\theta = 60°$ and ratio between curvature radius r and track width w of $r/w = 3.6$ permitted stretching of 14.4% before track breakage. For $r/w = 11.7$ a maximum elongation at break of 19.7% was measured. Larger opening angles θ provided even better flexibility but with increasing θ, the tensile strength and the electrical conductance of a single track is compromised and the maximum integration density (tracks per area) decreases.**

I. Introduction

Multi-channel electrode arrays are a common tool used by clinicians and researchers, providing an electrical interface to the nervous system. Numerous technologies have been developed over the past decades that allow fabrication of electrode arrays at high integration density and large channel count. Especially, when a specific biomedical application demands very high mechanical flexibility and/or large number of electrodes on a very small area, the integration of interconnection tracks that electrically link the electrode sites to wires or connectors is recommended. Integration in this context means that electrode sites and tracks are fabricated in the same process step and embedded in the same insulating substrate. The integrated tracks move the usually bulky interconnection area, where cables are welded or bonded to the electrodes further away from the delicate electrode sites and adjacent neural tissue. Alternatively, wires have to be attached to each electrode site individually, making the electrode array bulky and stiff.

The work presented here addresses the subject of integrated tracks in multi-electrode arrays fabricated from platinum foil (electrode sites, tracks and contact pads) and silicone rubber (insulating substrate) [1], a technology developed and used in our laboratories. Those electrode arrays are very flexible in a sense that they can easily be bent. However, longitudinal stretching is impeded by the metal tracks that cannot extend. Even the bending ability might be limited when more than one layer of metal tracks is present [2]. In this particular situation, some tracks might face compression forces; others tension forces, as shown in Fig. 1.

A few concepts are established that can potentially be applied to obtain stretchable and compressible integrated tracks. These concepts include the use of metal thin-film deposited on stretched silicone rubber, which is released before further processing, allowing an elongation of integrated tracks by up to 22% [3]. Other groups have used micro-channels filled with a liquid conductor [4]. One can also imagine the use of a metal or carbon filled elastomer as track material which is dispensed onto the substrate, improving flexibility over rigid metal tracks.

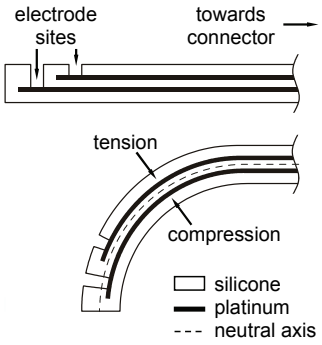

Fig. 1: Cross section of a double-layer electrode array: planar as processed (top) and bent (bottom). Bending causes tension and compression in the metal that cannot be compensated for, resulting in wrinkling or tearing of the metal layers.

An option that can be integrated most easily into the existing fabrication technology is to design the metal tracks in a meander-like way and therefore allow a certain stretch ability. Meander-shaped tracks have already been investigated by other groups [5] who found the horse-shoe superior over sinusoidal or U-shaped designs. Their findings encouraged us to apply the horse-shoe meander shape to the tracks of our neural electrodes in order to gain more flexibility. In this paper we evaluate the influence of the actual shape of the horse-shoe on the maximum elongation of the tracks, their tensile strength, the increase of pitch p (centre-to-centre distance) between two adjacent tracks, and the increase in track resistance based on experimental data and calculations.

Manuscript received April 23, 2009.

All Authors except P. Woias are with the Laboratory for Biomedical Microtechnology, Dept. of Microsystems Engineering - IMTEK, University of Freiburg, Germany (schuettler@ieee.org). P. Woias is heading the Laboratory for Design of Microsystems, IMTEK, University of Freiburg.

II. Materials and Methods

A. Mechanical Properties

The two materials used for the fabrication of neural electrode arrays according to our technology are high-purity platinum foil (99.95% Pt, Goodfellow, Friedberg, Germany) and medical grade silicone rubber MED-1000 (Nusil, Carpinteria, CA, USA). According to the suppliers, these two materials have very different mechanical properties, as shown in Table 1.

TABLE I
Material Properties of Silicone and Platinum

Property	MED-1000	99.95% Pt
Tensile Strength	6.2·Pa	200-300 MPa
Young's Modulus	0.8·MPa	170 GPa
Elongation at Break	600%	*not specified*

B. Design of Meander-Tracks

The horse-shoe design (Fig. 2) is described by the width w of the tracks, the minimum distance d between two adjacent tracks of the pitch p, the radius r, and the opening angle θ, which defines the curvature.

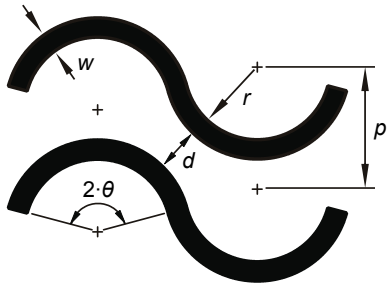

Fig. 2: Two adjacent meander-tracks and the parameters describing them.

In order to investigate the effect of the parameters θ for a selection of values for r and d on the maximal elongation before break, we fabricated samples of different designs, each of them consisting of multiple individual tracks (pitch p) that can be electrically interfaced by contact pads at both ends.

$$p = \sqrt{(2r+2w+d)^2 - (2r+w)^2 \cdot \sin^2(\theta)} - (2r+w)\cdot\cos(\theta) \qquad \text{Eq. 1}$$

Samples with a track width of $w = 86$ µm and radii of $r = 1007$ µm and r = 307 µm with opening angles θ of 0°, 30°, 60°, and 90° were fabricated. The pitch p, which minimal value can be calculated using Eq. 1 was set to 400 µm or larger; the shortest distance d between two tracks was set to 114 µm. An example of the design of such a sample is shown in Fig. 3.

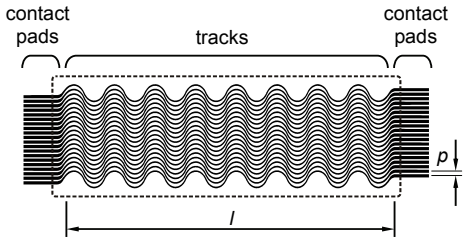

Fig. 3: Layout of a sample with 20 tracks arranged in a pitch p, opening angle $\theta = 60°$, $r = 1007$ µm. The dotted line indicates the area of silicone rubber. The actually stretched region has the length l.

C. Fabrication Process

The fabrication process is a variation of the basic process described in detail in [1], with an additional lift-off process step, as introduced in [6].

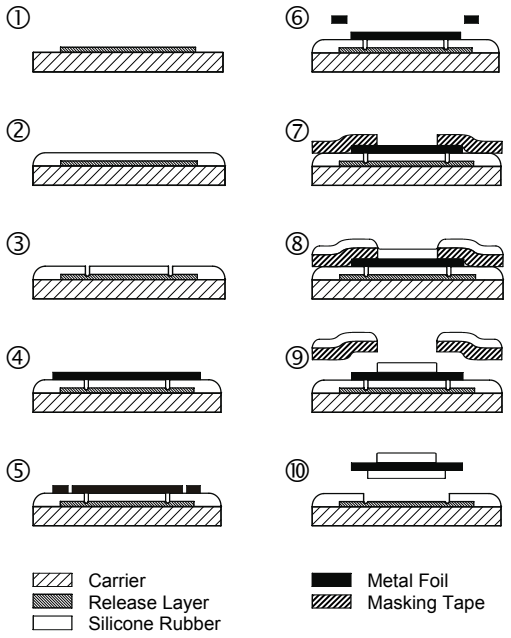

Fig. 4: Fabrication steps for silicone-embedded platinum tracks, applying lift-off technique.

A microscope glass slide is used as mechanical carrier during the fabrication process. Self adhesive tape (No 4124, tesa AG, Hamburg, Germany) is laminated to the carrier (Fig. 4-1). The tape acts as release layer to which a 20 µm thin layer of heptane-diluted MED-1000 silicone is spun-on (Fig. 4-2) using a standard spin-coater. The silicone adheres very well to the glass carrier but established only a very week bond to the tape. The rubber is patterend by a Nd:YAG marking laser (DPL Genesis Marker, cab, Karlsruhe, Germany) as shown in Fig. 4-3. Platinum foil of 12.5 µm thickness laminated to the silicone (Fig. 4-4) and

the perimeters of tracks and contact pads are laser-ablated (Fig. 4-5). After manually removing excess platinum foil (Fig. 4-6), masking tape (type 5413 Kapton® tape, 3M, Neuss, Germany) is applied at the locations of the contact pads at both ends of the tracks. A covering layer of diluted silicone rubber is spun on (Fig. 4-8). The masking tape is lifted-off: the metal contacts are exposed (Fig. 4-9). Now, the carrier is removed (Fig. 4-10) and the metal contacts of the silicone-metal-silicone sandwich are soldered to copper-clad printed circuit boards (PCBs).

D. Mechanical Tests

A multi-purpose bond-tester (type 4000 tester with WP10kg measurement cartridge, Dage, Aylesbury, Buckinghamshire, UK) stretched the samples with a velocity of $v = 50$ µm/s while the pull force was recorded. The electrical continuity of each track of a sample was monitored as well as possible electrical shorts between two adjacent tracks. The stretching of a sampled was stopped when all tracks were broken. The breakage of the tracks provided records of elongation at break and tensile strength, of which the average and the standard deviation were calculated. In order to reduce the error introduced by the pull-force of the silicone rubber, this force was subtracted from the original recordings before the data was analysed. Therefore, the rubber-induced force was calculated based on measurements of MED-1000 Young's modulus as a function of elongation, which was found to be non-linear (in contrast to the information from the supplier's datasheet).

III. Results

The fabricated samples had a total layer thickness of about 150 µm. Two of them, already assembled to PCB adapters, are shown in Fig. 5. Seven different designs were evaluated, and the elongation at break determined. All samples were pulled until every track was broken. Shorting of two adjacent tracks as response to the pull test was not observed.

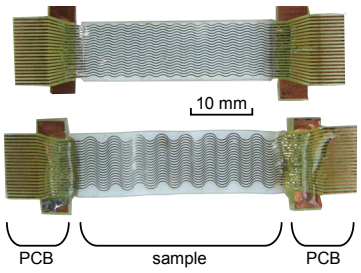

Fig. 5: Two test samples with and $r = 1007$ µm and opening angles $\theta = 30°$ (top) and 60° (bottom), soldered to PCB adapters.

Fig. 6 shows the measured elongation at break of the platinum tracks after minimizing the influence of the rubber: Tracks with larger radius are better stretchable than tracks with a smaller radius. With greater opening angle θ, this effect becomes more prominent. On average, straight tracks broke at 0.96% elongation, while at $\theta = 60°$, the tracks broke at 14.4% ($r = 307$ µm) and 19.7% ($r = 1007$ µm).

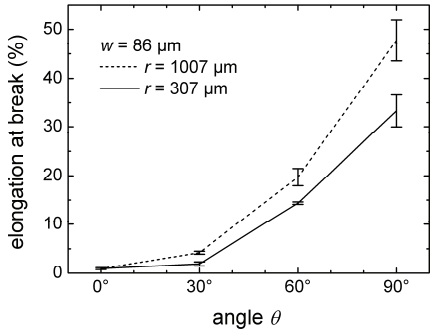

Fig. 6: Measured elongation at break for seven samples of different designs as a function of opening angle θ.

The tensile strength of straight tracks was measured to be 673 mN. For both radii the tracks became weaker with increasing opening angle θ. The tensile strength dropped below 160 mN at $\theta = 30°$. At $\theta = 60°$ the tracks with larger radius broke at 114 mN and the smaller radius tracks failed at 51 mN (Fig. 7).

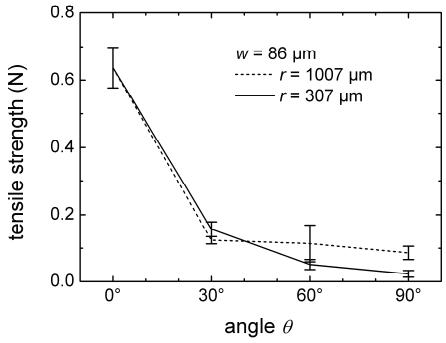

Fig. 7: Measured tensile strength for seven samples of different designs as a function of opening angle θ.

With increasing opening angle θ, the minimal pitch between two adjacent tracks increases. Fig. 8 shows the pitch calculated using Eq. 1 for four different designs. While straight tracks of width $w = 86$ µm and minimal distance $d = 114$ µm can be arranged at a pitch of $p = 200$ µm, meander-like tracks need additional space. The smallest pitch for $r = 307$ µm is $p = 315$ µm and for $r = 1007$ µm is $p = 358$ µm, at an angle of $\theta = 60°$. It has been shown in an earlier publication [7] that the laser technology permits a minimum track width of $w = 20$ µm at a distance $d = 60$ µm. Keeping the r/w ratio roughly similar to the sample design described before, the straight track pitch is 80 µm and the pitch at $\theta = 60°$ is $p = 114$ µm for a radius of $r = 60$ µm and $p = 133$ µm for $r = 200$ µm.

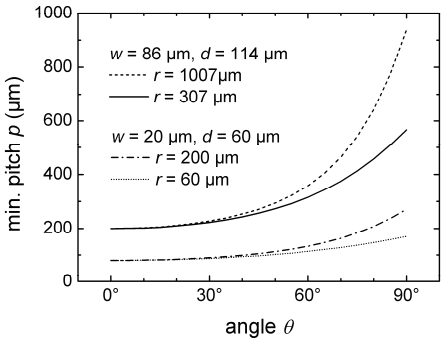

Fig. 8: Dependency of min. pitch from opening angle θ for four different track geometries.

The meander-shape causes the tracks to be effectively longer compared to straight tracks bridging the same distance l. A lengthening factor is calculated as a ratio of the effective length L of a meander track divided by the bridged length l. This factor L/l develops progressively with an increasing angle θ to values of 1.1 ($\theta = 30°$), 1.2 ($\theta = 60°$), and 1.6 ($\theta = 90°$) as plotted in Fig. 9

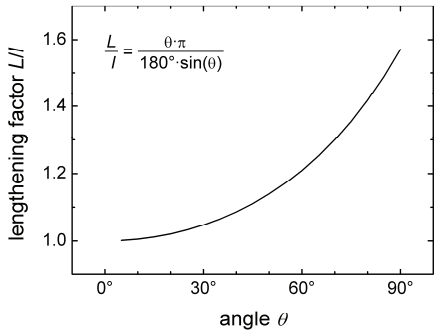

Fig. 9: Length L of a meander track relative to the actually bridged distance l as a function of meander opening angle θ.

IV. Discussion

Our experiments were carried out using simple electrical continuity tests. However, already before a meander track fails conducting, the development of little cracks can be observed, which are assumed to be early detectable by electrical resistivity measurements, which might give a better indication for the onset of failures during mechanical stress. This method would also deliver an experimental evaluation of the assumption that the lengthening factor L/l can be used to predict the increase of the electrical resistance R_M of a meander track relative to a straight track R_S of identical width w, using the equation $R_M = L/l \cdot R_S$.
The seven different samples evaluated in this work provide only a limited insight into the mechanical properties of a large range of possible horse-shoe designs. Based on the parameters $r/w = 3$, $\theta = 60°$, an electrode array was laser-fabricated (Fig. 10) which predecessors suffered from limited flexibility due to straight tracks. The new design provides the electrode array with a much better flexibility. It still needs to be proven that the reliability of this array is not compromised by the reduced tensile strength of the tracks.

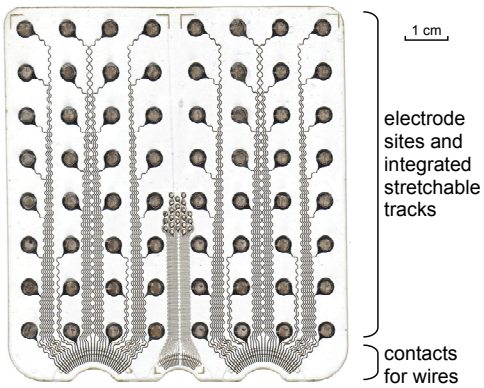

Fig. 10: A laser-fabricated ultra-flexible electrode array made for recording of electro-corticograms in large animals and humans.

V. Conclusion

A meander-like design provides flexibility to integrated tracks. However, the gained advantage has to be paid for by decreased integration density, dramatic reduction of track tensile strength, and moderate increase of tracks electrical resistivity.

References

[1] M. Schuettler, S. Stiess, B. King, G. J. Suaning, "Fabrication of implantable microelectrode arrays by laser-cutting of silicone rubber and platinum foil". *Journal of Neural Engineering*, No. 2, p. 121-128, 2005.

[2] G. J. Suaning, M. Schuettler, J. S. Ordonez, N. H. Lovell, N. H.: "Fabrication of Multi-Layer, High Density Micro-Electrode Arrays for Neural Stimulation and Bio-Signal Recording", *Proceedings of the IEEE Neural Engineering Conference*, pp. 5-8, 2007.

[3] S. P. Lacour, S. Wagner, Z. Huang, and Z. Suo, "Stretchable gold conductors on elastomeric substrates," *Applied Physics Letters*, vol. 82, no. 15, pp. 2404-2406, 2003.

[4] H. Kim, C. Son, and B. Ziaie, "Multi-axial super-stretchable interconnect with active electronics," *Proceedings of the 21st MEMS conference*, pp. 828-831, 2008.

[5] M. Gonzalez, F. Axisa, M. Vanden Bulcke, D. Brosteaux, B. Vandevelde, J. Vanfleteren, "Design of Metal Interconnects for Strechable Electronic Circuits using Finite Element Analysis", *Proceedings of EuroSimE,* pp. 110-115, 2007.

[6] M. Schuettler, J. S. Ordonez, C. Henle, D. Oh, O. Gilad, D. S. Holder, "A Flexible 29 Channel Epicortical Electrode Array". *Proceeding of the 13th Annual Conference of the International Functional Electrical Stimulation Society*, pp. 232-234, 2008.

[7] C. Henle, M. Schuettler, J. S. Ordonez, T. Stieglitz, T., "Scaling Limitations of Laser-Fabricated Nerve Electrode Arrays", *Proceedings of the IEEE EMBC Annual International* Conference, pp. 4208-4211, 2008.